Current Sheet Formation in a Conical Theta Pinch Faraday Accelerator with Radio-frequency Assisted Discharge

Ashley K. Hallock* and Edgar Y. Choueiri†
Princeton University, Princeton, NJ, 08544

Kurt A. Polzin‡
NASA - Marshall Space Flight Center, Huntsville, Alabama, 35812

Data from an inductive conical theta pinch accelerator are presented to gain insight into the process of inductive current sheet formation in the presence of a preionized background gas produced by a steady-state RF-discharge. The presence of a preionized plasma has been previously shown to allow for current sheet formation at lower discharge voltages and energies than those found in other pulsed inductive accelerator concepts, leading to greater accelerator efficiencies at lower power levels. Time-resolved magnetic probe measurements are obtained for different background pressures and pulse energies to characterize the effects of these parameters on current sheet formation. Indices are defined that describe time-resolved current sheet characteristics, such as the total current flowing in the current sheet, the time-integrated total current ("strength"), and current sheet velocity. It is found that for a given electric field strength, maximums in total current, strength, and velocity occur for one particular background pressure. At other pressures, these current sheet indices are considerably smaller. The trends observed in these indices are explained in terms of the principles behind Townsend breakdown that lead to a dependence on the ratio of the electric field to the background pressure. Time-integrated photographic data are also obtained at the same experimental conditions, and qualitatively they compare quite favorably with the time-resolved magnetic field data.

Nomenclature

$\mathbf{B}$	Magnetic field, T	t	time, μs
$\mathbf{E}$	Electric field, V/m	v	velocity, km/s
e	elementary charge, C	ϵ	energy, J
I	Current, A	λ	electron-neutral mean free path, m
$\mathbf{j}, j_\theta$	Current density, A/mm^2	μ_0	Permeability of vacuum, N/A^2
m_e	electron mass, kg	ν_m	momentum transfer collision frequency, s^{-1}
n_n	neutral density, m^{-3}	θ	angle from cone surface, degrees
p	pressure, mtorr	σ	conductivity, (ohm-m)$^{-1}$
S	Strength, A-μs	σ_m	electron-neutral collision cross section, m^2

*Graduate Student, Mechanical and Aerospace Engineering Department, E-Quad Olden St. Princeton, NJ 08544, Student Member AIAA.

†Chief Scientist of the Electric Propulsion and Plasma Dynamics Lab (EPPDyL) and Professor, Mechanical and Aerospace Engineering Department, E-Quad Olden St. Princeton, NJ 08544, Associate Fellow AIAA

‡Propulsion Research Engineer, Propulsion Research and Technology Applications Branch,Propulsion Systems Department, Senior Member AIAA.

I. Introduction

Pulsed inductive thrusters[1] are a specific class of electrodeless thrusters under development for use in space propulsion applications. Electrodeless thrusters are attractive due to their avoidance of the lifetime-limiting issues associated with electrode erosion. In addition, they can process propellants such as CO_2 and H_2O that are incompatible with metallic electrodes. These thrusters operate by discharging a short, high-current pulse through an inductive coil, producing a time-changing magnetic field that induces an electric field in accordance with Faraday's law. The propellant breaks down (ionizes) near the inductive coil, where the induced fields are sufficiently strong, and a current sheet forms with current flowing in the opposite direction to that of the current in the inductive coil. The proximity of the opposing current loops creates a high magnetic pressure between the plasma current sheet and the inductive coil, which accelerates the current sheet and any entrained propellant away from the coil to produce thrust. In Fig. 1 are two separate axisymmetric magnetostatic simulations (performed using Maxwell SV, Ansoft Corp.) of an inductive thruster that has a conical inductive coil, with an idealized driving current flowing azimuthally in one direction (orange) and an idealized mirror current flowing in the opposite direction (blue).

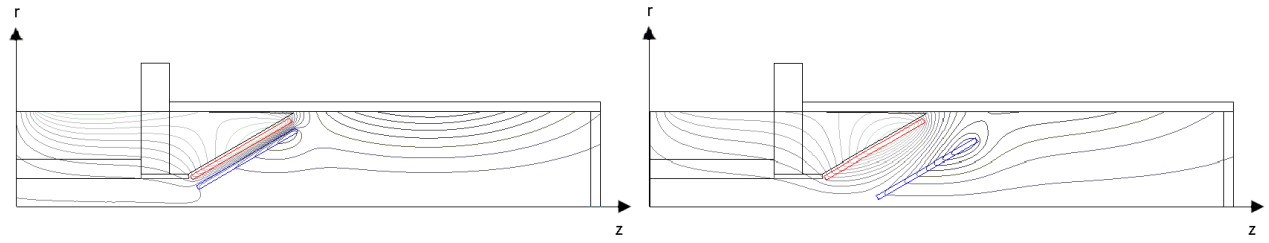

Figure 1. ***Left:*** **Magnetostatic simulation result showing a high magnetic pressure between the inductive coil (orange) and a current sheet (blue).** ***Right:*** **Magnetostatic simulation performed at a time after the current sheet has moved away from the inductive coil.**

Figure 1 can be viewed as two snapshots in time giving a comparison of the magnetic pressure between the coil and current sheet for two separate sheet locations. The further the current sheet is from the inductive coil, the lower the magnetic pressure. Slow current sheet formation can produce a resistive plasma that doesn't effectively entrain propellant. This also leads to energy losses in radiated fields and ohmic heating losses as the current pulse rings in the driving circuit. One way to increase the speed of current sheet formation is through the use of a preionized propellant.[2] Choueiri and Polzin[3] introduced the Faraday Accelerator with Radio-frequency Assisted Discharge (FARAD) to demonstrate the concept of preioniation-assisted low discharge energy inductive current sheet formation. They have performed proof-of-concept experiments, developed design criteria,[4] and identified potential advantages a FARAD thruster might enjoy over the current state-of-the-art Pulsed Inductive Thruster (PIT).[1,5,6] Although the use of preionization adds complexity to the system, it can also help to eliminate complexity elsewhere, yielding a system that is, on balance, simpler and more compact. The proof-of-concept experiments were successful in demonstrating preionization-assisted current sheet formation at significantly lower capacitor voltages and pulse energies than those found in the PIT (1.5 kV and 44J versus 30kV and 4kJ). In previous FARAD experiments, propellant reached the flat inductive coil surface from a preionization chamber located upstream of the coil. This required the use of a strongly cusped magnetic field to impose a ninety degree turn on the preionized propellant stream. Turning the propellant was a relatively difficult process and it served to motivate the design of an inductive coil that more naturally follows the diffusive path of the preionized gas, resulting in the Conical Theta Pinch FARAD.[7] The CTP coil geometry is the sole difference between CTP-FARAD and the original FARAD proof-of-concept experiments.

The efficiency of pulsed inductive plasma thrusters depends greatly on the current sheet's ability to contain the magnetic field. There is an advantage for pulsed inductive thrusters where the current sheet has a high total current and forms close to the inductive acceleration coil, as this maximizes both the field strength as well as the interaction between the field and the current sheet. While there are many other current sheet characteristics that affect the performance of the thruster (e.g. sheet extent, propellant leakage, stability), the present study focuses on the current sheet's total current and time-varying position. Knowing the conditions under which the strongest current sheet forms (with respect to the above sheet characteristics), and possessing an understanding of the effect various controllable parameters have on current sheet formation

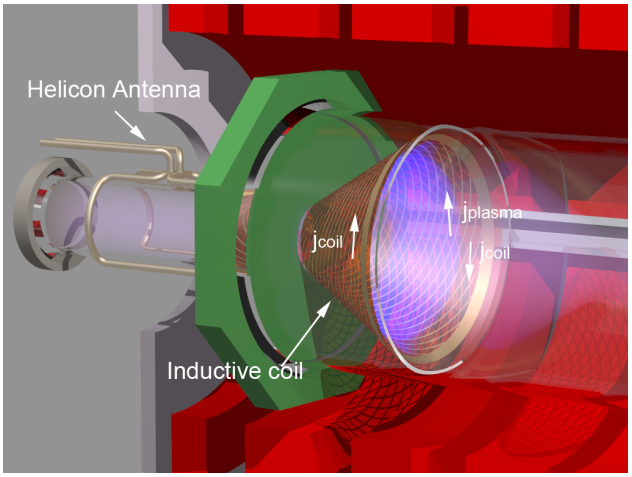

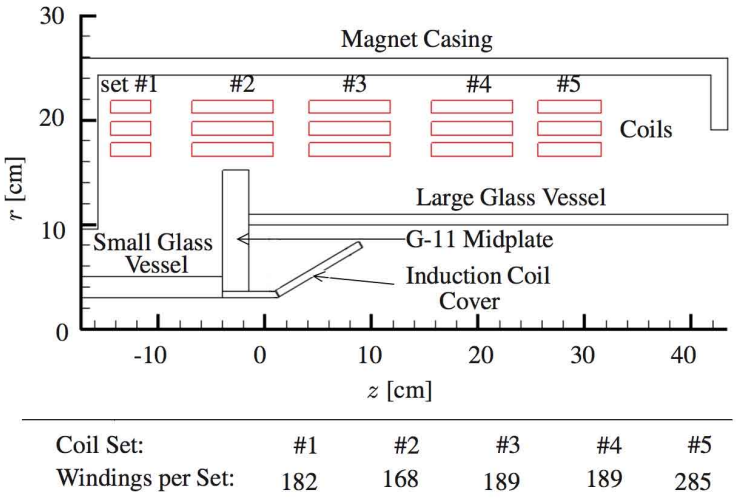

Coil Set:	#1	#2	#3	#4	#5
Windings per Set:	182	168	189	189	285

Figure 2. ***Top:*** **Schematic of CTP FARAD and** ***Bottom:*** **the geometry of the axisymmetric applied magnetic field model.[8]**

and acceleration are useful in guiding the selection of operating conditions of future designs.

A previous photographic study[7] found that there is an optimal pressure at which the most intense current sheet forms. This study lacked time-resolved measurements of the current sheet formation process, leaving many important questions regarding the motion of the current sheet unanswered. The goal of the present study is to present time-resolved current density measurements to evaluate the total current, strength, and velocity of the current sheet and demonstrate its dependence on experimentally controllable parameters. These direct measurements are compared to previously-acquired photographic data to check for inconsistencies between the two measurements. To simplify the experiment, propellant is loaded as an ambient backfill (as opposed to employing a more complex propellant injection method that could be used in a space thruster). This helps isolate the current sheet formation process from other gas-dynamic effects associated with propellant injection and expansion. These contours are numerically integrated over the cross sectional area of the current sheet to calculate the total current as a function of time. In addition, we use these data to find the velocity of the centroid of current density at different backfill pressure conditions while holding all other experimentally controllable parameters fixed.

The remainder of this paper is organized into successive sections in which we describe the experiment, report time-resolved current density measurements, discuss the observed trends and use these trends to extract physical insight into some of the basic mechanisms controlling the current sheet formation process.

II. Experimental Setup

A. Vacuum Chamber

All experiments were performed in a vacuum chamber consisting of two pyrex cylinders joined together by a fiberglass plate onto which a pyrex funnel supporting the CTP inductive circuit is mounted, extending 12 cm into the larger cylinder. The smaller cylinder has an inner diameter of 6 cm and is 37 cm long and the larger cylinder has an inner diameter of 20 cm and is 46 cm long. While the experiment can be operated with mass injection through the endplate of the smaller cylinder, an ambient backfill technique is used in these experiments. The pressure is monitored using a Granville Phillips 275 mini-convectron pressure gauge. Plasma is created in the smaller, preionization chamber and is guided by an applied magnetic field through a 6 cm inner diameter concentric hole in the fiberglass plate into the region bounded by the CTP supporting cone. A 150 l/s turbomolecular pump backed by a roughing pump is attached to the larger cylinder at the endplate opposite to the CTP inductive coil; the same endplate where gas is fed into the vacuum vessel.

B. Plasma Source

A Boswell-type saddle antenna is wrapped around the smaller cylinder, creating the preionization chamber. The saddle is composed of quarter-inch copper tubing attached to a water cooling line. An ENI 13.56 MHz 1.25 kW power supply is coupled to the antenna through a tuner consisting of two Jennings 1000 pF 3kV variable vacuum capacitors located immediately next to the antenna and used to minimize reflected power. A Faraday cage surrounds the entire experiment to shield from radiated RF fields. All experiments are performed at 1.25 kW forward power with 30 W reflected (representing the upper power limit of the supply and the best possible match with the tuner, respectively).

C. Applied Magnetic Field

A Varian VA-1955A klystron magnet surrounds the vacuum vessel and provides an applied magnetic field. The magnet is composed of five separate, water-cooled coils that are connected to two separate Electronic Measurements EMCC 120-40 power supplies, allowing the current in coils 1 and 2 to flow in one direction, and the current through coils 3, 4 and 5 in an opposite direction (coils are labeled in Fig. 2). The current through these groups of coils can be varied independently, allowing a range of magnetic field configurations.

The use of a 2-D axisymmetric numerical model (Maxwell SV, by Ansoft Corp.) to calculate the magnetic field profiles for various values of current through the five sets of coils has been previously validated.[8] Calculation results for the applied magnetic field profile used in the experiments described here are shown in Fig. 3. These results correspond to the case where 15 amps are flowing through coil sets 1 and 2, and 10 amps are flowing through coil sets 3, 4 and 5. The experiments described in this paper were performed using the applied magnetic field configuration shown in fig. 3. This field configuration was chosen because it represents conditions under which stronger current sheet formation was observed.

The applied magnetic field is useful because it can increase the current density in the current sheet by increasing the plasma density of the preionized propellant at the coil face. The angle through which the plasma must turn after leaving the RF antenna is greatly decreased from the case of a flat inductive coil. Unlike in the FARAD proof of concept experiment, a current sheet can be formed without the presence of an applied magnetic field, however in the experiments described below an applied magnetic field is used because it was found to increase the current density in the current sheet.

D. Conical Theta Pinch

The conical theta pinch is composed of a flexible circuit board wrapped around a pyrex funnel with a wall thickness of 4 mm that provides structural support to the circuit board. The neck of the funnel, with a 6 cm inner diameter and 2 cm length, fits into the concentric hole in the fiberglass plate holding the funnel's axis parallel to the horizontal plane. The conical coil used for the present study has a half-angle of 30 degrees, and has previously been described in detail.[7]

Current is fed to the coil through strip-lines that run between a 39.2μF capacitor and the current feed point of the inductive coil. The circuit penetrates the vacuum vessel through metal standoffs, which connect two sections of the stripline. The current pulse is initiated (as in FARAD) using a "hammer" switch. When the current pulse flows through the inductive coil, a time changing magnetic field is produced with radial and

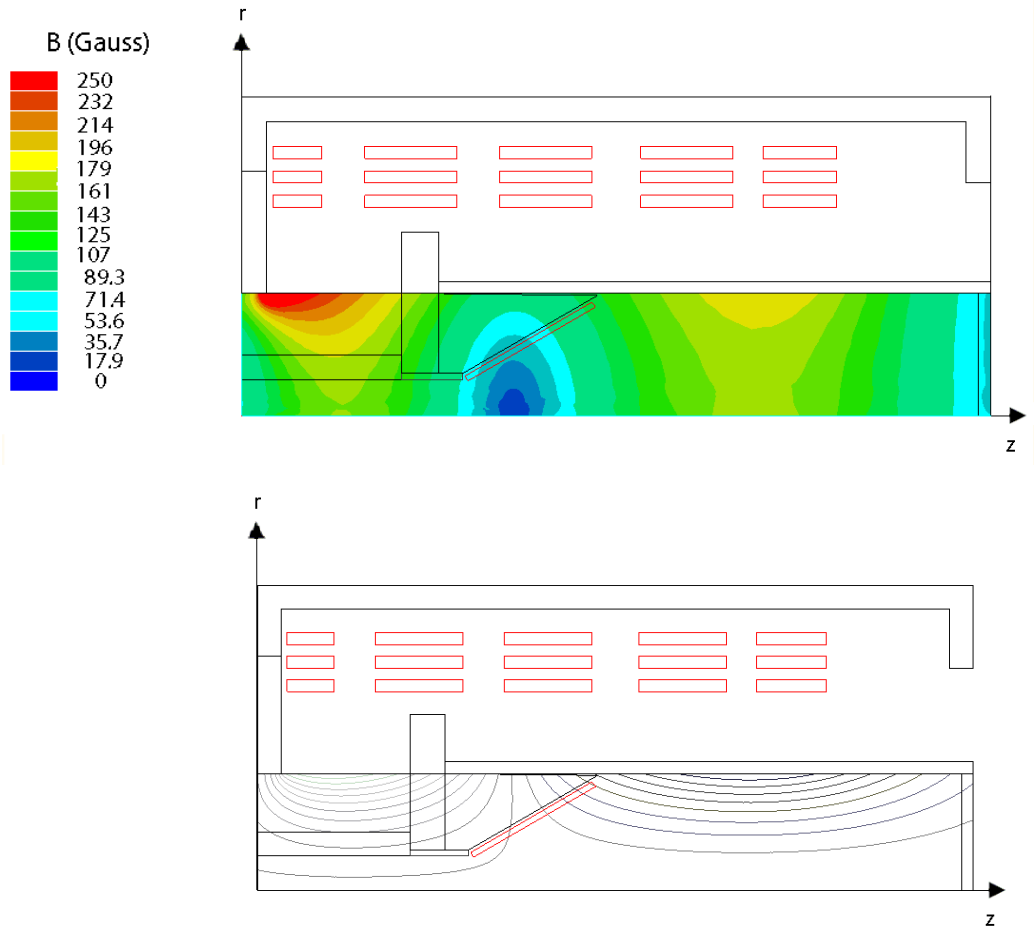

Figure 3. *Top:* **Applied magnetic field simulation and** *Bottom:* **flux lines for the case of 15 Amps flowing through coils 1 and 2, and 10 Amps flowing through coils 3, 4 and 5.**

axial components that induces an azimuthal electric field in the volume contained by the coil. Preionization of the propellant allows for current sheet formation during the first half cycle of the pulse at voltage levels an order of magnitude lower than those required for operation of the PIT.[3] The magnetic field generated by the current sheet partially cancels the field from the inductive coil downstream of the sheet, and adds to the coil's magnetic field upstream of the sheet. This increases the magnetic pressure between the inductive coil and current sheet, and acts to accelerate the sheet away from the coil. Schematics showing the idealized stages of sheet formation and acceleration can be found in Fig. 4.

E. Time-integrated Photography

A Nikon D50 digital SLR camera with a 50 mm focal length lens was used to capture time-integrated images of the luminous pattern associated with the current sheet. All automatic compensations for light intensity, gamma, and color balance were defeated in the acquisition of these data. Each picture has a one second exposure time and was obtained using an ISO of 200, and an 8x neutral density filter. The camera was positioned for a top view of the cone at a distance of roughly 60 cm from the cone exit. Due to physical constraints of the experimental setup, the camera is unable to view the cone surface at an angle where the "film plane" of the camera is parallel to the plane subtending the bottom edge of the cone. All photographs were obtained with an angle of 30 degrees between these two planes. The position of the camera relative to the inductive coil is shown in Fig. 5.

The picture frame includes the lower half of the interior surface of the cone, allowing for visual determination of the intensity and extent of the luminous structure from the cone's inlet to its outlet. The aperture

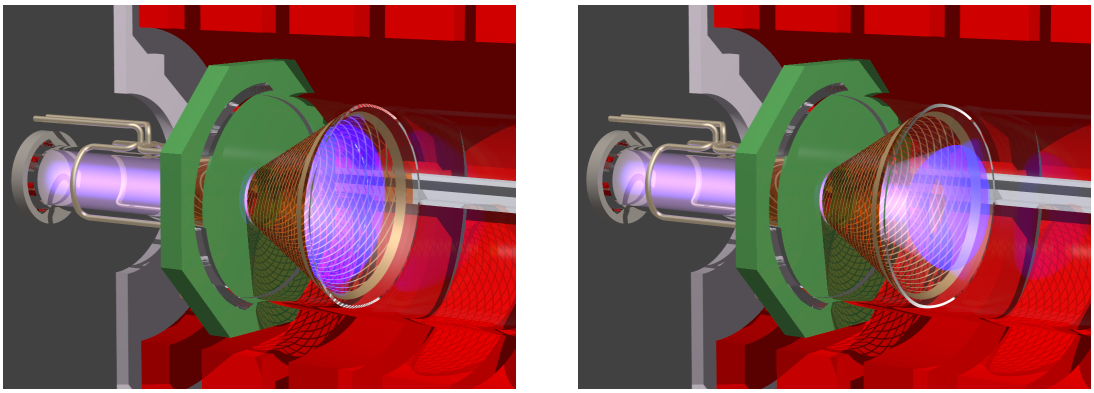

Figure 4. Idealized schematics showing current sheet formation (left panel) and pinching (right panel) in the CTP-FARAD. The current sheet (shown in blue) forms near the inner surface of the inductive coil, and is accelerated away from the coil (radially and axially) by a Lorentz force caused by the interaction between the current sheet and the magnetic field.

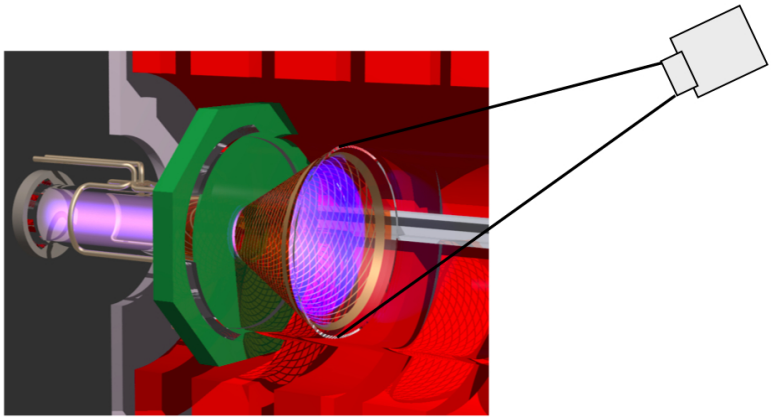

Figure 5. The position of the camera with respect to the inductive coil.

is remotely opened and closes automatically after one second has elapsed.

F. Time-varying Magnetic Field Measurements

The time-varying magnetic fields within the volume of the inductive coil are measured using a three-axis B-dot probe. This probe is a simple arrangement of three mutually perpendicular surface mount chip inductors. A voltage across any one of the three inductor terminals is directly proportional to the time rate of change of the magnetic field, and the signal can be integrated to yield all components of the magnetic field at the location of the probe. A more detailed description of the physics of B-dot probes can be found in Ref. [9].

The probe constructed for this experiment consisted of three air core 220 nH chip inductors oriented perpendicular to each other to provide resolvability in a three-dimensional coordinate system. The signal from each of the inductors passes through a center-tapped transformer, providing common-mode signal rejection. The probe is movable, and can be placed at any axial or radial position within the volume enclosed by the CTP coil. The signal is numerically integrated to yield the magnetic field profile at a given spatial location inside the CTP coil as a function of time.

G. Current Density Measurements

The measurements of the magnetic field in the two-dimensional r-z plane allow for computation of the current density using Ampère's law,

$$\nabla \times \mathbf{B} = \mu_0 \mathbf{j}.$$

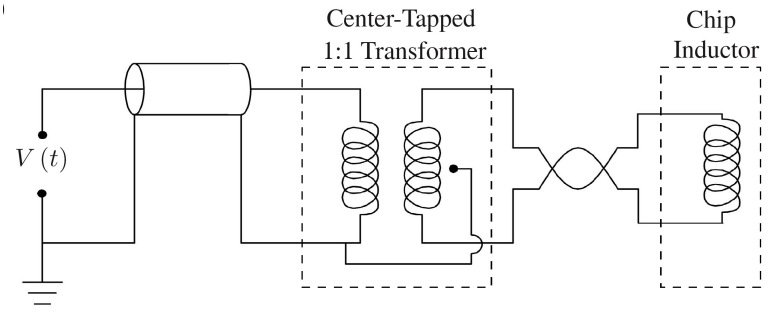

Figure 6. Balanced circuit for the B-dot probe.[8]

This technique works because the only portion of the magnetic field in the region of interest that is not curl free is attributable to the current sheet. To calculate the curl, magnetic field data were taken at 98 different locations in a region within and adjacent to the CTP coil. Data were obtained on an r-z grid and are assumed to be azimuthally symmetric due to the uniformity of current sheet images in the azimuthal direction. These data were used in MatLab to produce animations that show the temporal evolution of the current density.

III. Experimental Results

Data were obtained at various pressures between 16 and 63 mtorr for two different capacitor voltages (V_c = 2 kV, 1.5 kV). The preionization stage was operated at a forward RF power level of 1.25 kW, which is the maximum output of the RF power supply. The tuner was adjusted so that only 30 W of RF power were reflected. The applied magnetic field was never changed from the configuration shown in Fig. 3. B-dot probe data were obtained on an r-z grid and used to calculate both the induced electric field and the current density as a function of radial location, axial location and time. The current density was then numerically integrated over r and z to give a measure of the total plasma current, and it was subsequently numerically integrated in time to give a measure of the total current sheet strength. The centroid of the current sheet cross section is calculated from the contours and used to find the centroid velocity, initial location, and temporal evolution.

A. Time-resolved Current Sheet Cross-Section Contours

B-dot probe data were obtained over an r-z grid composed of 98 locations: 14 axial stations each having 7 radial stations. The grid extends axially in equal intervals of 0.6 cm for a total length of 7.8 cm along the inductive coil. The grid extends radially inward from the coil face and is evenly spaced in intervals of 0.35 cm. This distance is sufficient to record current sheet movement away from the cone. No significant current density levels were found outside of this range in either the axial or radial directions. These data were converted into contours and compiled into animations showing the time evolution of the current sheet cross section. Contours are presented in Fig. 7 for one specific instant in time and show the current sheet's position relative to the location of the inductive coil. As an example, three frames showing the time-evolution of the current sheet for a backfill pressure of 32 mtorr and a capacitor voltage of 2 kV are presented in Fig. 8.

B. Induced Electric Field

The induced electric field can be calculated from the B-dot probe signal using Faraday's law:

$$\nabla \times \mathbf{E} = -\frac{\partial \mathbf{B}}{\partial t}$$

The calculation is performed at each location in the r-z spatial grid, and the field values are spatially averaged to obtain a single electric field value for each experimental case. The electric field is mainly a function of the capacitor voltage, changing only slightly as the background pressure is varied. The change in electric

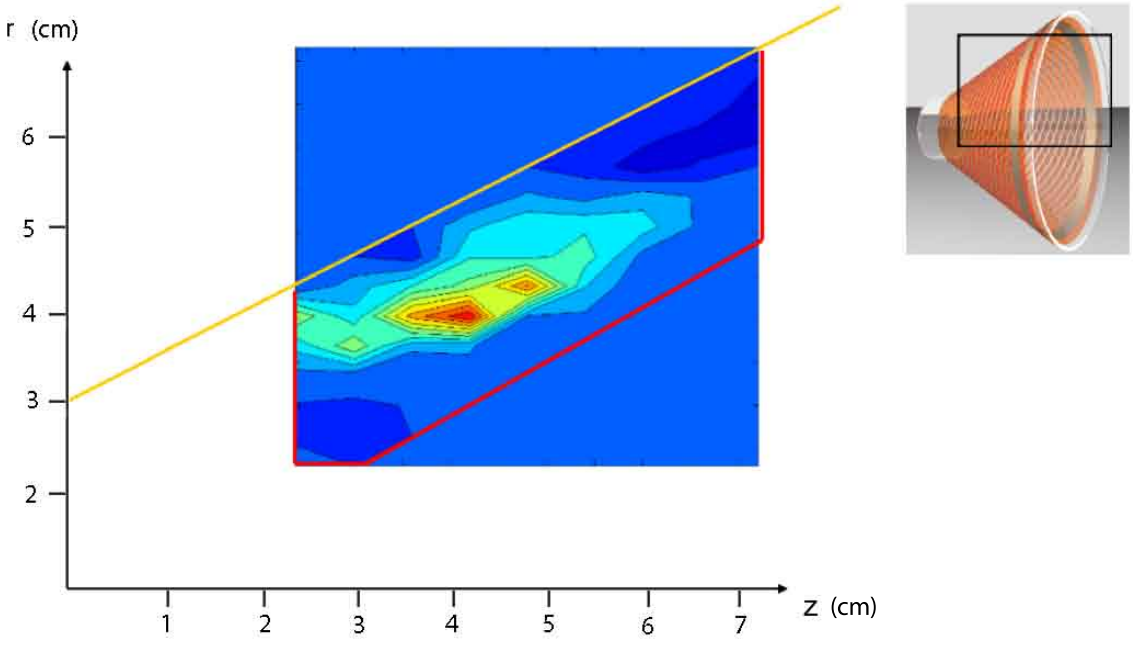

Figure 7. The contours are taken over an r-z grid within the volume of the cone. The location (0,0) coincides with the center of the smaller end of the cone where the cone mounts onto the fiberglass plate. The z-axis is the axis of symmetry. In the graph, the orange line represents the inductive coil mounted on the cone, and the red outlined area represents the area where data were taken.

field with pressure for the case where $V_c = 2$ kV is shown in Fig. 9. The electric field traces for different pressures are averaged for each capacitor voltage to compare the electric field strengths for the case of $V_c = 2$ kV and $V_c = 1.5$ kV, and a comparison is shown in Fig. 10. The average electric field from the time when the induced field overpowers the RF field to the time when the current sheet begins to move away from the inductive coil is 170 ± 5 V/m for $V_c = 2$ kV and 129 ± 3 for $V_c = 1.5$ kV. The time period over which the electric field is averaged is the same for all experimental conditions.

C. Total Plasma Current

The total plasma current (I) is calculated as the integral of the current density over the area of the current sheet,

$$I(t) = \int \int j_\theta(r, z, t) dr dz.$$

Calculated curves of I versus time are shown for different backfill pressures and capacitor voltages in Fig. 11. For the case of $V_c = 2$ kV, the plot shows that the maximum total plasma current during the discharge is highest for a pressure of 32 mtorr, whereas for $V_c = 1.5$ kV, the maximum total plasma current is highest for a pressure of 24 mtorr. In addition, these graphs show that the initial current rise rate in the sheet is highest and the maximum in plasma current is reached fastest at the lowest pressure. The initial current rise rates for different pressures and electric field strengths are shown in Tables 1 and 2, and the times at which the total plasma current reaches a maximum for different pressures and electric field strengths are shown in Tables 3 and 4. The rise rates are calculated using data from the time when the discharge starts to a time 0.088 μs later. The current rise rate decreases and the time at which the maximum plasma current is reached (or the "peak time") increases with increasing pressure.

D. Strength

Since the total plasma current varies in time, another index we define is a parameter we call "strength". The strength (S) of the current sheet is defined as the integral over time of the total plasma current flowing

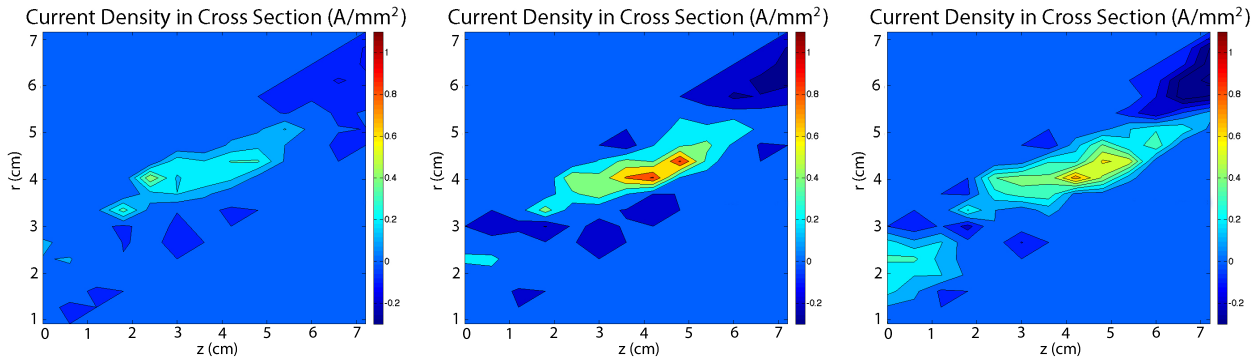

Figure 8. Three frames from a current sheet cross section animation taken at a pressure of 32 mtorr and a capacitor voltage of 2 kV with an applied magnetic field. The frames correspond to (from left to right) .5 μs, 1 μs, and 1.5 μs into the discharge.

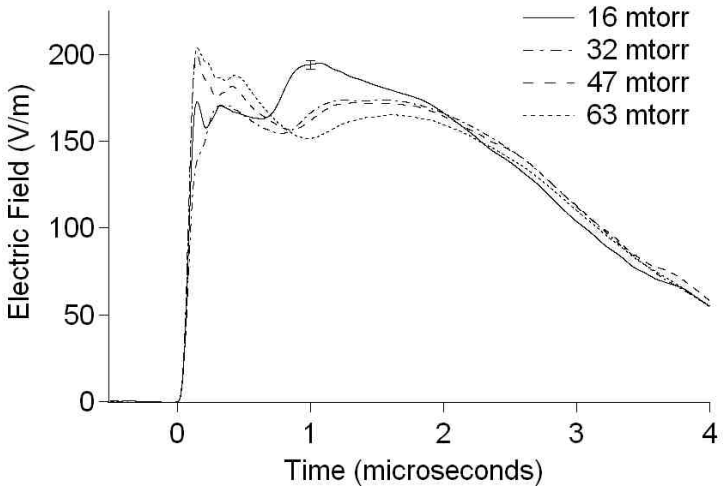

Figure 9. Calculated electric field averaged over the B-dot probe spatial grid for various pressures at V_c = 2 kV, shown with a typical error bar.

through the sheet,

$$S = \int I dt.$$

This calculation gives a measure of the total amount of plasma current over the duration of the discharge. The strengths of current sheets at different pressures for $V_c = 1.5$ kV and 2 kV are shown in Tables 5 and 6.

For a fixed discharge voltage, there is clearly an optimum pressure at which the strength of the current sheet is maximized. At a given voltage, the maximum sheet strength and maximum total plasma current occur at the same pressure, and this pressure changes with changing capacitor voltage. It appears that the parameter of greatest importance in determining the optimum conditions for current sheet formation is the ratio of the induced electric field to the background pressure. For $V_c = 2$ kV, the strongest current sheet forms when $E/p \approx 170/32 = 5.3$ V/mtorr/m and for $V_c = 1.5$ kV, the strongest sheet forms when $E/p \approx 129/24 = 5.4$ V/mtorr/m. The difference between these two values is smaller than their respective error bars. In the next section, we proceed to investigate the effect of pressure on the acceleration of the current sheet.

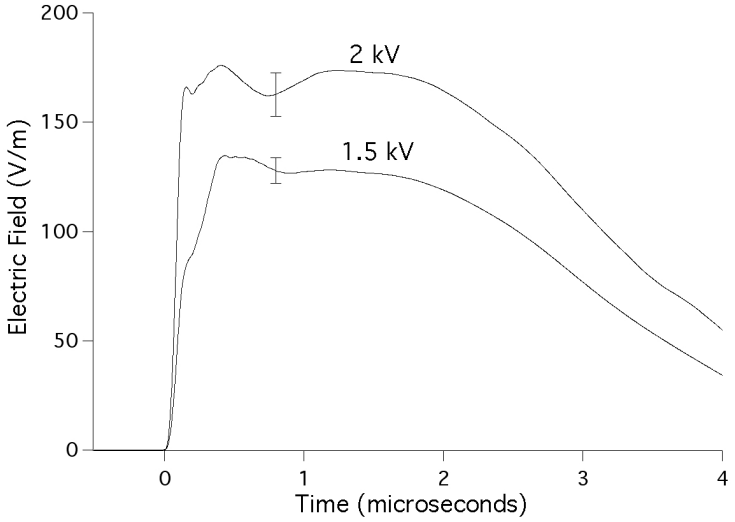

Figure 10. Calculated electric field averaged over the B-dot probe spatial grid and averaged over various pressures at V_c = 2 kV and 1.5 kV, shown with a typical error bar.

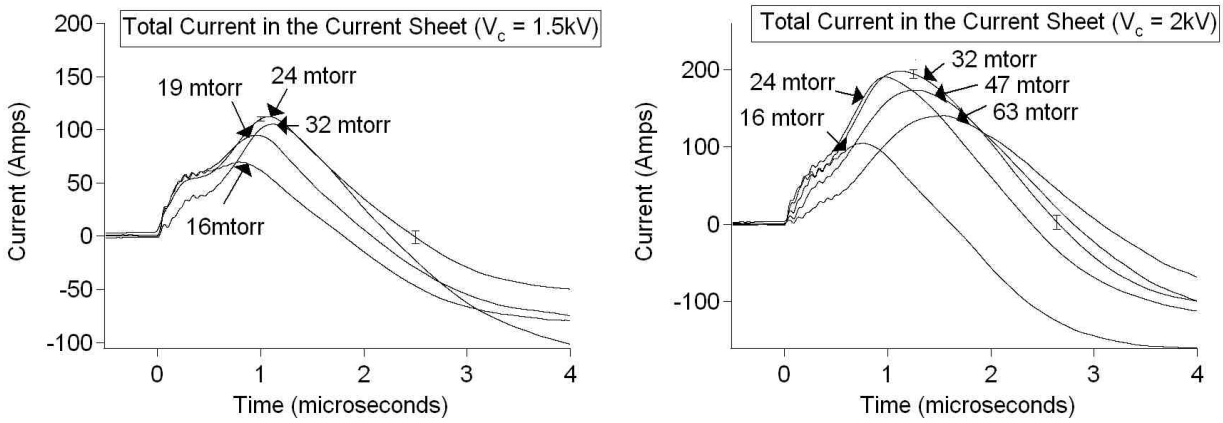

Figure 11. Total current flowing in the current sheet for different values of backfill pressure at *Top:* V_c = 1.5 kV, and *Bottom:* V_c = 2 kV.

E. Current Sheet Centroid Velocity

The speed of the current sheet is characterized by tracking the motion of the sheet's centroid (computed for a cross section defined by an r-z plane). The average current sheet speed is calculated by taking the time-of-flight from the location where the sheet forms and begins moving (r_1, z_1), and where the sheet stops and dissolves (r_2, z_2), and is given by:

$$v = \frac{\sqrt{r_2^2 + z_2^2} - \sqrt{r_1^2 + z_1^2}}{t_2 - t_1}.$$

At V_c = 2 kV, the only pressure for which a velocity measurement could be made was 32 mtorr, the result being 6.7 km/s ± 1.9 km/s with an angle (θ) from the cone of 65.8 degrees (shown in Fig. 12). Because the velocity measurements for all other pressures were significantly lower, there is therefore a clear maximum in centroid velocity (for V_c = 2kV) occurring near 32 mtorr. This is also the condition where the total plasma current and sheet strength were maximized. No velocity calculations are presented for any other conditions because the measurements in those cases all had error bars that were larger than the measurements themselves.

Table 1. Total Plasma Current Initial Rise Rates for V_c = 1.5 kV, $E \approx 129$ V/m

p (mtorr)	dI/dt (A/μs)
16	294 ± 30
19	233 ± 24
24	190 ± 18
32	53 ± 5

Table 2. Total Plasma Current Initial Rise Rates for V_c = 2 kV, $E \approx 170$ V/m

p (mtorr)	dI/dt (A/μs)
16	329 ± 60
24	270 ± 49
32	186 ± 34
47	67 ± 12
63	8 ± 2

Table 3. "Peak Times" for V_c = 1.5 kV, $E \approx 129$ V/m

p (mtorr)	t (μs)
16	.786 ± .02
19	.954 ± .02
24	1.08 ± .01
32	1.12 ± .05

Table 4. "Peak Times" for V_c = 2 kV, $E \approx 170$ V/m

p (mtorr)	t (μs)
16	.742 ± .05
24	1.08 ± .05
32	1.12 ± .02
47	1.28 ± .04
63	1.46 ± .12

F. Formation Position along the Inductive Coil

The centroid is used to calculate the formation position along the inductive coil. The formation position is the time-averaged location of the current sheet from the time the induced electric field begins to dominate the RF field to the time when the centroid either begins to move or the current sheet dissolves (if no movement is observed). The formation position as a function of pressure is shown in Fig. 13, with the distance along the CTP surface measured from the upstream end near the preionization chamber. The current sheet forms closer to the upstream end of the inductive coil as the pressure is increased.

IV. Discussion

In this section we address some of the underlying physical mechanisms leading to the trends observed in the previous section. An exression for the average electron energy gain from the electric field between collisions is used to explain the effect of background pressure and the induced electric field on both the maximum in current sheet strength and in total plasma current. A circuit model of the thruster is used to explain the trends in current density initial rise rate and formation position along the inductive coil. Results from direct current density measurements are compared with previous photographic measurements to establish the latter's effectiveness as a diagnostic technique.

A. Optimum E/p Ratio for Current Sheet Formation

The current arising in the current sheet in the presence of the induced electric field depends on the conductivity of the preionized plasma near the inner surface of the inductive coil. Electrons in the preionized propellant are accelerated azimuthally by the induced electric field of the inductive coil. Because the frequency of the electric field ($\sim$ 100 kHz) is much smaller than the electron plasma frequency ($\sim$ 1 GHz) or the electron cyclotron frequency ($\sim$ 100 MHz), the field can be assumed constant with respect to the electron dynamics, jutsifying the use of a DC conductivity expression for the preionized propellant:

$$\sigma = \frac{n_e e^2}{m_e \nu_m}$$

Due to the low ionization fraction, the only significant increase in conductivity will be caused by an inrease in the electron number density during the acceleration pulse.

Table 5. Current Sheet Strengths for V_c = 1.5 kV

p (mtorr)	S (A-μs)
16	57 ± 3
19	70 ± 4
24	72 ± 4
32	53 ± 3

Table 6. Current Sheet Strengths for V_c = 2 kV

p (mtorr)	S (A-μs)
16	89 ± 12
24	122 ± 14
32	210 ± 110
47	100 ± 10
63	76 ± 22

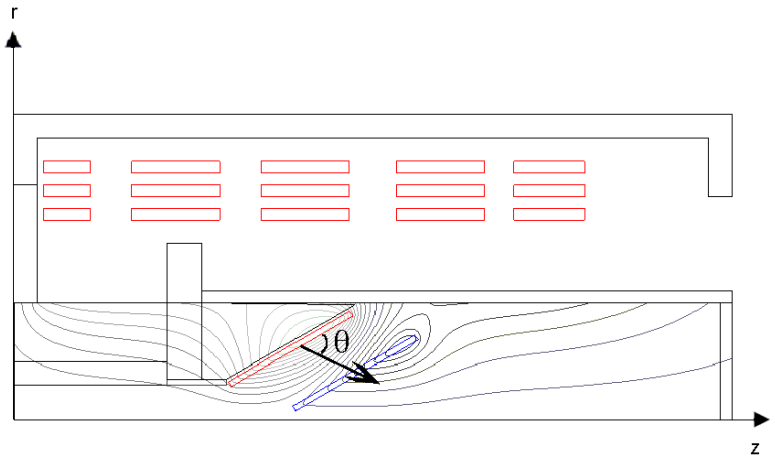

Figure 12. Schematic showing the displacement of the cross-sectional current density centroid.

The energy (ϵ) gained from the induced electric field by electrons in the plasma depends upon the strength of the electric field and the distance the electrons travel between momentum-randomizing collisions. This distance (the electron-neutral mean free path, λ) is inversely proportional to the pressure:

$$\lambda = \frac{1}{n_n \sigma_m}.$$

If we assume that the temperature is constant during the discharge, then the number density varies linearly with the background pressure. The longer an electron's mean free path, the greater the amount of kinetic energy it can gain from the field. This implies that the electron energy gain between collisions is directly proportional to the electric field and inversely proportional to the pressure,

$$\epsilon \propto E\lambda \propto E/(n_n \sigma_m) \propto f(E/p).$$

The dominant ionization process in a weakly ionized, low temperature plasma is electron-impact ionization.[10] The electrons in the plasma are assumed to be Maxwellian, with a temperature of 2.5 eV.[8] At this temperature, the energy added by the electric field always increases the electrons' ability to ionize neutrals over the range of pulse energies and background pressures considered here, and this energy increases with increasing induced electric field. Consequently, the ionization rate (and also the conductivity) of the plasma in the presence of the induced electric field must be a function of E/p.

B. Effect of Inductive Circuit on Current Sheet Formation

The accelerator and plasma can be electrically represented as the lump-element circuit model shown in Fig. 14. The resistivity of a weakly ionized plasma, such as the background RF-produced plasma in CTP-FARAD, is dominated by electron-neutral collisions. As the pressure is increased, the frequency of these collisions increases, causing a commensurate rise in the preionized plasma's resistivity. During the inductive

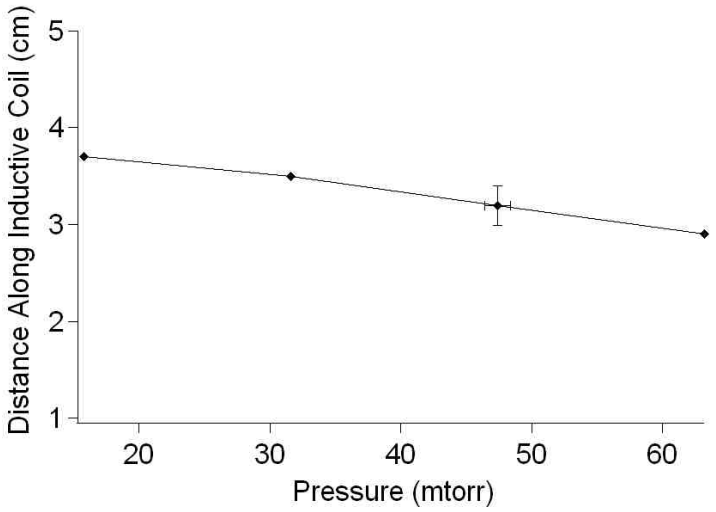

Figure 13. The formation distance along the inductive coil as a function of pressure shown with a typical error bar.

pulse, the plasma has a resistance R_p that is roughly equal to the resistivity integrated around the mean circumference of the current sheet. If we assume the current sheet forms against the inner surface of the theta-pinch coil at a specific axial location, we can see that the plasma resistance associated with this position increases with pressure (same path length, greater collisionality). At a fixed pressure, we also note that the plasma resistance decreases as the current sheet formation position moves axially towards the inlet of the theta-pinch coil (same collisionality, shorter path length). From a circuit point-of-view, illustrated in Fig. 14, we recognize that the voltage drop across the plasma side of the transformer must be equal to the voltage drop owing to the plasma resistance. This implies that the current sheet must form further upstream in the theta-pinch coil as the pressure is increased. Consequently, in a pulsed inductive discharge the sheet may be forced to form at a location other than the point that minimizes the overall circuit inductance. The rising resistance in the plasma with increasing pressure also reduces the initial current rise rate, causing plasma currents at higher pressures to initially lag behind those at lower pressures. The effects of ionization greatly overwhelm this initial advantage within the first microsecond with respect to the maximum total current achieved and the total current sheet strength, however the maximum in total current is shifted to later times for higher pressures.

C. Comparison with Previous Photographic Experiments

Previous time-integrated photographic data[7] revealed that there exists an optimum pressure for the total intensity of light measured along the surface of the inductive coil. This observation has been confirmed by the present study where it was shown that there is a clear maximum in both current sheet strength and velocity as a function of induced electric field and pressure. Photographic data were obtained at a charge voltage V_c

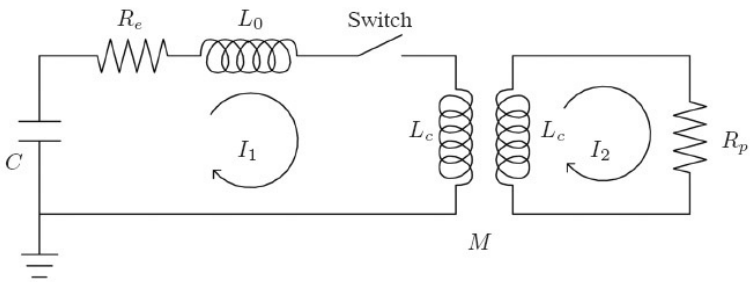

Figure 14. Schematic of the thruster as an inductive circuit, after Ref. [11].

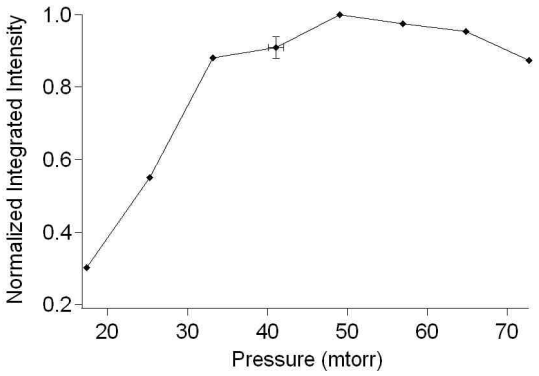

Figure 15. Normalized integrated intensity as a function of background pressure performed at the same experimental conditions as the magnetic probe experiments for V_c = 2 kV, shown with a typical error bar.

= 2 kV, and can be directly compared to the measured current density data presented in this paper. The integrated intensities of light emitted by the current sheet at different background pressure levels normalized to the maximum observed integrated intensity are presented in Fig. 15. These data were calculated following the method described in Ref. 7. While the pressure at which the maximum light intensity was recorded is higher than the pressure at which the maximum total plasma current, maximum current sheet strength and maximum centroid velocity were measured, the existence of an optimum pressure is clear in the photographic data.

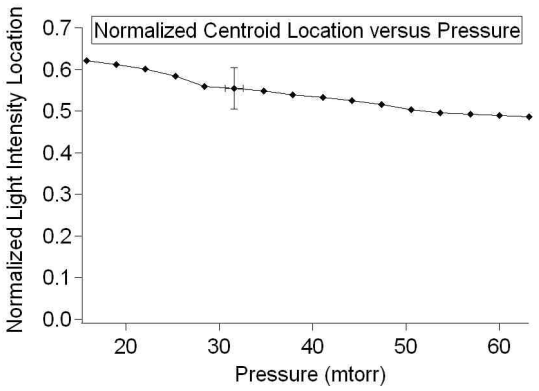

Figure 16. Normalized centroid location as a function of background pressure at the same operating conditions as the magnetic probe experiment described in the previous section, shown with a typical error bar.

It is reasonable that the photographs would not coincide with direct current density measurements, because the light intensity is time-integrated and not necessarily originating from current density. The time response of the camera could bias intensity measurements of current sheets depending on their movement, possibly recording lower intensities for a current sheet with higher current density due to its higher velocity. It has been shown that light intensity can be a good indication of the presence of current density,[12] and so we make further comparisons of the two types of experiments to determine if light intensity data can predict other trends observed in current density data. Using light intensity data from the experiment performed at the same operating conditions as the B-dot probe experiments, the centroid of the light intensity was calculated, and is shown in Fig. 16. This graph shows the light intensity centroid location normalized with respect to the cone exit located 13.5 cm from the cone inlet. This shows the current sheet forming around 6-7 cm from the upstream end of the inductive coil while Fig. 13 shows the current sheet forming at a distance of between 3 and 4 cm. Both plots agree in showing the current sheet moving upstream with increasing pressure.

Yet another trend replicated in photographic data is the critical E/p ratio noted in subsections C, D, and E of section III. Photographic experimental results performed at two different charge voltages where the background pressure was varied are presented in Fig. 17. Unlike the B-dot probe measurements, these

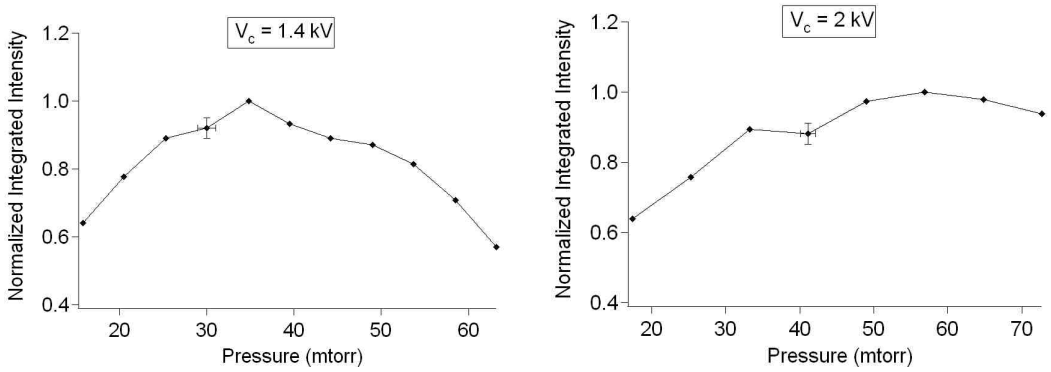

Figure 17. Time-integrated experimental data showing a relationship between integrated current sheet light intensity and the ratio of E/p. The figures show light intensity data for *Left:* V_c = 1.4 kV and *Right:* V_c = 2 kV, shown with typical error bars.

experiments were performed without the use of an applied magnetic field. The observed change in optimum pressure for a change in V_c (or induced electric field) is shown in these plots, and within the error bars the highest normalized integrated intensity occurs at the same ratio of the electric field to background pressure for these two photographic experiments.

V. Conclusions

Both time-resolved magnetic probe and time-integrated photographic measurements of current sheet formation have been made in the CTP FARAD for a range of background pressures and capacitor voltages. The results of these measurements indicate that there are optimal conditions for current sheet formation that depend on both the induced electric field and the background pressure. The strongest current sheet, measured by both spatially and time-integrated plasma current density in the current sheet, occurs at a constant ratio of the electric field to the background pressure. The highest velocity also occurs under these same conditions, while at other conditions the velocity is significantly reduced. The dependence on the ratio E/p is reasonable considering the Townsend-like breakdown process occurring during current sheet formation and the DC conductivity of the preionized plasma. The initial current rise rate in the sheet decreases with increasing pressure because the plasma resistivity increases with increasing pressure, which from a circuit point of view will affect the time rate-of-change in the plasma current. This change in initial rise rate affects how long the current sheet will spend climbing to the maximum total plasma current, but the dominance of the Townsend-like ionization process leads to a dependence of the value of the maximum total plasma current and the maximum strength on the ratio E/p. Comparison with previous photographic, time-integrated data shows inconsistency with respect to absolute values for centroid location and optimum E/p ratio, however the centroid location trend persists and the existence of a critical E/p ratio is present in both types of measurements.

Acknowledgments

This research project is carried out under a contract from the the Air Force Office of Scientific Research. We also acknowledge support from the Plasma Science and Technology Program from the Princeton Plasma Physics Laboratory. We thank Mr. Robert Sorenson for his valuable technical support and for the 3-D illustrations of the CTP-FARAD concept.

References

[1]C.L.Dailey and R.H. Lovberg. Large diameter inductive plasma thrusters. Number AIAA 79-2093, oct 1979.

[2]R. G. Jahn. *Physics of Electric Propulsion.* McGraw-Hill Book Company, 1968.

[3]E. Y. Choueiri and K. A. Polzin. Faraday Acceleration with Radio-frequency Assisted Discharge. *Journal of Propulsion and Power*, 22(3):611–619, May-June 2006.

[4]K. A. Polzin and E. Y. Choueiri. Performance optimization criteria for pulsed inductive plasma acceleration. *IEEE Transactions on Plasma Science*, 34(3):945–953, 2006.

[5]C.L. Dailey and R.H. Lovberg. Current sheet structure in an inductive-impulsive plasma accelerator. *AIAA Journal*, 10(2):125–192, Feb. 1972.

[6]R.H.Lovberg C.L.Dailey. PIT Mark V design. Number AIAA 91-3571, 1991.

[7]A. K. Hallock and E. Y. Choueiri. Current Sheet Formation in a Conical Theta Pinch Faraday Accelerator with Radio-frequency Assisted Discharge. Number IEPC-2007-165, September 2007.

[8]K. A. Polzin. *Faraday Accelerator with Radio-frequency Assisted Discharge (FARAD)*. Ph.d. dissertation, Princeton University, Department of Mechanical and Aerospace Engineering, 2006.

[9]R. H. Lovberg. Magnetic probes. In S. L. Leonard R. H. Huddlestone, editor, *Plasma Diagnostic Techniques*, pages 69–112. Academic Press, 1965.

[10]Y. P. Raizer. *Gas Discharge Physics*. Springer, 1991.

[11]R. H. Lovberg and C. L. Dailey. Large inductive thruster performance measurement. *AIAA*, 20(7):971, July 1982.

[12]T.E. Markusic and J. W. Berkery E. Y. Choueiri. Visualization of current sheet evolution in a pulsed plasma accelerator. *IEEE Transactions of Plasma Science*, 33(2):528–529, April 2005.